Research Article

ADVANCED PHOTONICS

Real-time measurement of non-Hermitian Landau–Zener tunneling near band crossings

Lange Zhao,[a,†] Shulin Wang,[a,b,†] Chengzhi Qin,[a,†] Bing Wang,[a,*] Han Ye,[a] Weiwei Liu,[a] Stefano Longhi,[c,d,*] and Peixiang Lu[a,e,*]

[a]Huazhong University of Science and Technology, Wuhan National Laboratory for Optoelectronics and School of Physics, Wuhan, China
[b]Southeast University, School of Physics, Nanjing, China
[c]Politecnico di Milano, Dipartimento di Fisica, Milano, Italy
[d]Instituto de Fisica Interdisciplinary Sistemas Complejos, IFISC (UIB-CSIC), Palma de Mallorca, Spain
[e]Wuhan Institute of Technology, Hubei Key Laboratory of Optical Information and Pattern Recognition, Wuhan, China

Abstract. Landau–Zener (LZ) tunneling, i.e., the nonadiabatic level transition under strong parameter driving, is a fundamental concept in modern quantum mechanics. With the advent of non-Hermitian physics, research interest has been paid to the LZ tunneling involving level dissipations. However, experimental demonstrations of such an interesting non-Hermitian LZ problem remain yet elusive. By harnessing a synthetic temporal lattice using a fiber-loop circuit, we report on the first real-time measurement of non-Hermitian LZ tunneling in a dissipative two-band lattice model. An innovative approach based on mode interference is developed to measure the transient band occupancies, providing a powerful tool to explore the non-Hermitian LZ tunneling dynamics in non-orthogonal eigenmodes. We find that the loss does not change the final LZ tunneling probability but can highly affect the tunneling process by modifying the typical band occupancies oscillation behaviors. We initiate exploring intriguing LZ physics and measurements beyond the standard Hermitian paradigm, with potential applications in coherent quantum control and quantum technologies.

Keywords: Landau–Zener tunneling; non-Hermitian physics; synthetic dimension.

Received Sep. 29, 2024; revised manuscript received Feb. 19, 2025; accepted for publication Feb. 27, 2025; published online Apr. 11, 2025.

© The Authors. Published by SPIE and CLP under a Creative Commons Attribution 4.0 International License. Distribution or reproduction of this work in whole or in part requires full attribution of the original publication, including its DOI.

[DOI: 10.1117/1.AP.7.3.036002]

1 Introduction

Landau–Zener (LZ) tunneling,[1–4] i.e., the nonadiabatic transition under strong parameter driving in multilevel quantum systems, is a fundamental phenomenon, which is at the heart of a plethora of important effects in different areas of physics. For example, in crystalline materials, LZ tunneling is responsible for interband transitions and transport of electrons under a strong DC electric field, whereas, in quantum electrodynamics, it explains the Schwinger effect of vacuum pair creation. It is also of particular interest in the context of quantum computing and quantum information processing, where precise control over quantum states and their transitions is crucial for implementing quantum algorithms and protocols.[4] LZ tunneling has been observed in various systems, such as in semiconductor superlattices,[5,6] cold atoms in optical lattices,[7,8] superconducting qubits,[9] optical waves in photonic lattices,[10,11] and acoustic waves in periodic media[12] to mention a few. The energy levels usually manifest a crossing on a diabatic basis and an avoided crossing on an adiabatic basis. Along with the transition probability, a related issue is the time it takes for the LZ process to occur.[3,13–15] On the experimental side, this problem remains challenging because it requires accurate measurements of the instantaneous dynamics in both diabatic and adiabatic bases, which have been so far achieved only partly.[16,17]

Recently, there has been a huge interest in quantum systems described by non-Hermitian Hamiltonians, which arise naturally in the description of open (dissipative) systems.[18–20] For example, Bloch oscillations in parity-time symmetric non-Hermitian systems have attracted much attention.[21–23] Several theoretical

*Address all correspondence to Bing Wang, wangbing@hust.edu.cn; Stefano Longhi, stefano.longhi@polimi.it; Peixiang Lu, lupeixiang@hust.edu.cn

†These authors contributed equally to this work.

studies have extended LZ tunneling to dissipative systems, revealing abundant physics[24–33] with several promising applications to, e.g., circuit quantum electrodynamics, molecular nanomagnets, and quantum computing.[27] Note that LZ tunneling concerns mode evolution between two different energy bands, which requires a stronger driving field.[34–36] In non-Hermitian systems, the eigenvalues are typically complex, and in parameter space, they can display a nontrivial topology related to the appearance of exceptional points (EPs),[37–40] where simultaneous coalescence of eigenenergies and corresponding eigenvectors occurs. In addition, in non-Hermitian systems, the eigenvectors are not orthogonal and adiabaticity can be fragile,[41,42] which could greatly impact level crossing dynamics. In a dissipative gapped two-band lattice model, the avoided level crossing in a complex energy plane can be described by a universal Dirac form of band structure with Lorentz-symmetry violation.[31,43] Such a complex two-band model is capable of describing the non-Hermitian skin effect in continuous models and displays a topological phase transition at the EP crossing.[31,44] Interestingly, in dissipative LZ tunneling, the transition probability coincides with the standard LZ formula of an isolated (Hermitian) two-level system,[24,27] even if we cross an EP. In spite of the great theoretical interest in non-Hermitian extensions of LZ tunneling, experimental observations of such fascinating regimes in systems with controlled dissipation remain so far elusive in quantum systems mainly because of the difficulty of engineering and controlling dissipative Hamiltonians in quantum materials and the ability to perform real-time measurements of level occupancies in both diabatic and adiabatic bases. Recently, synthetic optical lattices stemming from mode coupling in distinct dimensions, such as time,[45–53] frequency,[54–57] angular momentum,[58–60] and supermodes,[61] have provided fascinating platforms for the experimental observation of a wealth of lattice phenomena in synthetic dimension,[62] even beyond the Hermitian paradigm.[46,48,51,56,57]

In this work, we report on the experimental observation of LZ tunneling in a dissipative two-band lattice realized in synthetic optical temporal lattices and displaying a universal Dirac form with Lorentz-symmetry violation. An interferometric technique based on abrupt gauge potential shift is developed to accurately measure the transient band occupancies both in diabatic and adiabatic bases. Our results demonstrate one of the most surprising theoretical predictions of non-Hermitian LZ tunneling, namely, the independence of tunneling probability on the dissipation.[24,27] The loss can rather affect the transient tunneling process by speeding up the tunneling process and modifying the characteristic oscillation magnitude of band occupancies, which can also smear out the oscillation features at a loss rate large enough above EP. Our work introduces an innovative interferometric technique to characterize and control tunneling processes in quantum processes, demonstrating LZ physics beyond the Hermitian paradigm with potential applications to coherent quantum control and quantum technologies.[27]

Compared with previous studies, we emphasize that our study provides a well-conceived method to measure the tunneling probabilities in the vicinity of band crossings, where the modes have nearly identical velocities.[16,17] In addition, the temporal lattices here we used provide an excellent platform, which can not only demonstrate the non-Hermitian LZ tunneling effect but also control the process flexibly, enabling the measurement of the tunneling process in real time. Finally, the tunneling probabilities in diabatic and adiabatic bases are both experimentally presented, which reveals evidently the influence of non-Hermitian features on the tunneling process.

2 Results and Discussion

2.1 Realization of Non-Hermitian LZ Tunneling in Temporal Lattices

We realize a dissipative two-band lattice using time multiplexing of optical pulses in two coupled fiber loops with slightly different lengths, which are connected by an optical coupler with a tunable splitting ratio, as shown in Fig. 1(a). The slight length difference enables a relative time delay for individual pulses traveling in the loops. The time instants of all pulses in the fiber loops can be mapped into a synthetic mesh-type temporal lattice denoted by (n, m), as depicted in Note 1 in the Supplementary Material, where m is evolution step representing the roundtrip number of pulses in the two loops and n is the lattice site denoting the relative pulse position in each roundtrip. The pulse dynamics in the lattice is governed by the following evolution equations:[45–53]

$$\begin{cases} u_n^{m+1} = [\cos(\beta)u_{n+1}^m + i\,\sin(\beta)v_{n+1}^m]e^{i\phi(m)-\gamma} \\ v_n^{m+1} = [i\,\sin(\beta)u_{n-1}^m + \cos(\beta)v_{n-1}^m]e^{-i\phi(m)} \end{cases}, \tag{1}$$

where u_n^m and v_n^m denote the pulse amplitudes at position n and time step m in short and long loops, respectively, β is the coupling angle defining the splitting ratio of the variable optical coupler, $\phi(m)$ is the step-dependent phase modulation, and γ is the loss rate. The equations can be easily obtained by considering the coupling of each optical pulse between adjacent time steps when taking into account the phase and intensity modulations (detailed derivation in Note 2 in the Supplementary Material). The intensity modulator in the short loop allows us to introduce controllable loss γ into the lattice, which defines the imaginary part of the underlying potential. Phase modulators are utilized to induce phase shift $\phi(m)$ representing the real part of the potential. By imposing opposite phase modulations $\pm\phi(m)$ in the two fiber loops, we can get an effective vector potential $A = -\phi(m)$,[63,64] which corresponds to an effective electric field $E = -\mathrm{d}A/\mathrm{d}m$. The Bloch momentum thus experiences a linear drift $Q = Q_0 + \int_0^m E(\tau)\mathrm{d}\tau = Q_0 + \phi(m)$, where Q_0 stands for the initial Bloch momentum. The Bloch momentum in the lattice refers to the phase difference between adjacent optical pulses, which is controllable by the phase modulator. The instantaneous eigen Bloch modes and corresponding quasi-energies are obtained from Eq. (1) by making the ansatz $(u_n^m, v_n^m)^T = (U, V)^T e^{iQ_0 n} e^{i\theta m}$, where U and V denote the mode amplitudes in the short and long loops, and θ is the quasi energy. Substituting the eigen Bloch modes into Eq. (1), we get the eigenvalue equation $\Gamma(Q)(U, V)^T = e^{i\theta}(U, V)^T$ with

$$\Gamma(Q) = \begin{pmatrix} \cos(\beta)e^{iQ}e^{-\gamma} & i\,\sin(\beta)e^{iQ}e^{-\gamma} \\ i\,\sin(\beta)e^{-iQ} & \cos(\beta)e^{-iQ} \end{pmatrix}. \tag{2}$$

Note that, here, we take the value $Q = Q_0 + \phi(m)$. By solving the eigenvalue equation, the quasi-energy bands are obtained as

$$\theta_\pm = \pm\arccos\left[\cos(\beta)\cos\left(Q + i\frac{\gamma}{2}\right)\right] + i\frac{\gamma}{2}, \tag{3}$$

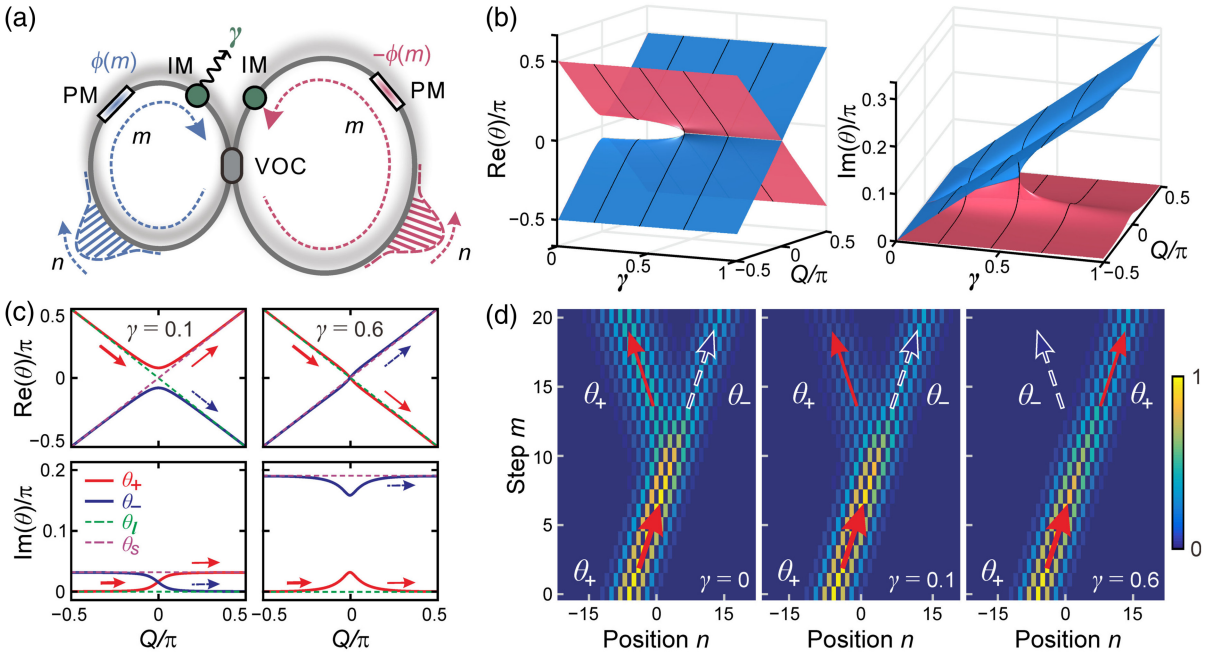

Fig. 1 Non-Hermitian LZ tunneling in synthetic temporal lattices. (a) Schematic diagram of two fiber loops connected by a variable optical coupler (VOC) for yielding synthetic temporal lattice. The phase modulations of $\pm\phi(m)$ are introduced in the short and long loops through phase modulators (PMs). The intensity modulator (IM) is utilized to introduce loss with the loss rate γ. (b) Complex eigenvalues (quasi energies) in the space spanned by Bloch momentum and loss rate. Here, $\sin^2(\beta) = 0.05$. Note the spectral phase transition at $\gamma = \gamma_c$. (c) Complex band structures for $\gamma = 0.1$ and 0.6. (d) Numerical results of pulse intensity (total intensity of the short and long loops) evolutions under a driving electric field $E = \pi/20$ for $\gamma = 0$, 0.1, and 0.6. The initial eigenmode is prepared at $Q_0 = -\pi/2$ and $\theta_+ = \pi/2$.

and the corresponding eigenmodes

$$|\varphi_\pm\rangle = \begin{pmatrix} U_\pm \\ V_\pm \end{pmatrix} = \frac{1}{\sqrt{1+|e^{\mp\lambda+\gamma/2}|}} \begin{pmatrix} 0 \\ \pm e^{\mp\lambda - iQ + \gamma/2} \end{pmatrix}, \tag{4}$$

where we have set $\lambda = \text{arcsinh}[\cot(\beta)\sin(Q + i\gamma/2)]$. Equations (2)–(4) hold true whether the phase modulation $\phi(m)$ is 0 or not. When the phase $\phi(m)$ is slowly ramped in time, that is, $\phi(m) = mE$ with $E \ll 1$, the Bloch momentum $Q = Q_0 + \phi(m)$ spans the Brillouin zone, and the eigenmodes in Eq. (4) can be employed as adiabatic bases when the system experiences adiabatic evolution. Note that they are not naturally orthogonal in non-Hermitian systems. The quasi-energies $\theta_\pm$ in the parameter space spanned by γ and Q are illustrated in Fig. 1(b). An EP appears at $Q = 0$ and $\gamma = \gamma_c$ with $\gamma_c = 2\,\text{arccosh}[1/\cos(\beta)]$, where the two energy bands and corresponding eigenmodes both coalesce with each other. In our experiment, the coupling angle is set such that $\sin^2(\beta) = 0.05$, corresponding to a critical loss rate $\gamma_c = 0.46$. Interestingly, near the band avoided crossing point $Q = 0$ and assuming a small coupling angle β and loss rate γ, the quasi energies approximately read

$$\theta_\pm = \pm\sqrt{\beta^2 + \left(Q + i\frac{\gamma}{2}\right)^2} + i\frac{\gamma}{2}, \tag{5}$$

which describe the canonical dispersion curves of a Dirac equation with Lorentz-symmetry violation,[31,44] featuring the non-Hermitian skin effect[48] and a spectral phase transition at the EP $\gamma = \gamma_c$.[26,44] Indeed, assuming small values of β and γ, the long-wavelength (continuous) limit of Eq. (1), corresponding to $Q \to 0$ near the crossing region, reduces to a non-Hermitian Dirac equation in Weyl representation with an imaginary gauge potential.[26,44]

As the loss rate increases from 0, the system undergoes a transition from weak ($\gamma \ll \gamma_c$) to strong ($\gamma \gg \gamma_c$) non-Hermiticity regimes,[65] for which we plot the real and imaginary parts of quasi-energies for two representative values $\gamma = 0.1$ and 0.6 in Fig. 1(c). The profiles of eigenmodes[66] can be found in Note 2 in the Supplementary Material. For a small loss rate γ, there is an avoided crossing of the real parts and a crossing of the imaginary parts at $Q = 0$. On the contrary, as γ increases beyond EP, the real parts form a crossing, whereas the imaginary parts form an avoided crossing still at $Q = 0$. Generally, the eigenmodes in Eq. (4) are usually referred to adiabatic bases, which can be written as the superposition of diabatic bases: $|\varphi_\pm\rangle = U_\pm|\varphi_s\rangle + V_\pm|\varphi_l\rangle$, where $|\varphi_s\rangle = (1,0)^T$ and $|\varphi_l\rangle = (0,1)^T$ are diabatic bases denoting the orthogonal bare modes in uncoupled short and long loops. The corresponding eigenvalues of diabatic basis are $\theta_s = Q + i\gamma$ and $\theta_l = -Q$ [denoted by the dashed lines in Fig. 1(c)], where real values experience a crossing at $Q = 0$.

Figure 1(d) shows the comparisons of simulated beam evolutions between traditional Hermitian LZ tunneling and non-

Hermitian LZ tunneling processes under different loss rates. Here, the tunneling probability is formulated in terms of the diabatic basis.[4] As we excite from the diabatic basis $|\varphi_l\rangle$ at remote time $t \to -\infty$, the tunneling probability is thus denoted by the residual packet staying in the same $|\varphi_l\rangle$ mode at final time $t \to \infty$. By comparing the three cases, we can find that the residual packet as denoted by the rightward output beam remains unchanged as γ varies, indicating that non-Hermiticity does not change the final tunneling probability, even when we cross EP. By contrast, in terms of adiabatic basis, the tunneled part is represented by the rightward beam (θ_+) as $\gamma < \gamma_c$ (central panel) and leftward one (θ_-) as $\gamma > \gamma_c$ (right panel). For the traditional Hermitian LZ tunneling process (left panel), the packet manifests a clear beam splitting at band crossing, giving rise to two undamped beam branches. For non-Hermitian LZ tunneling processes, the leftward beam branch experiences a clear damping, whereas the rightward one remains undamped (central and right panels). The reason why the rightward beam remains unchanged as γ varies is that the loss is added only into the short loop, such that the mode $|\varphi_s\rangle$ is always lossy and decays faster than mode $|\varphi_l\rangle$ in the long loop. Although the presence of loss does not alter the final LZ tunneling probability, it will greatly influence the LZ tunneling process, as we shall demonstrate below.

2.2 Measurement of Non-Hermitian LZ Tunneling Process

To reveal how the non-Hermiticity controls the non-Hermitian LZ tunneling dynamics, we propose a stepwise quench scheme to indirectly measure the whole tunneling process. Specifically, we first truncate the tunneling by suddenly removing the effective electric field and optical loss, thereby freezing the band occupancies. From the subsequent pattern of mode interference, we can readily extract the desirable band occupancies. By truncating the LZ tunneling step by step, the whole LZ tunneling process can hence be measured. To display our quench scheme, we depict the band structures for truncating steps $m_t = 10$ and $m_t = 12$ in Fig. 2(a) and plot the required gauge potentials and effective electric fields in Fig. 2(b). Here, we set the coupling and electric field as $\sin^2(\beta) = 0.05$ and $E = \pi/20$, respectively, and choose the loss as $\gamma = 0.1$. One can see that, at the band crossing point $m_t = 10$, the two modes in different bands have identical group velocities and become indistinguishable. As a consequence, the two modes overlap entirely after the truncation and exhibit a perfect interference. For other truncating steps near the crossing, say $m_t = 12$, the two modes have slightly different group velocities, and the interference fades out, as illustrated in Fig. 2(c). To handle this problem, we perform an abrupt phase

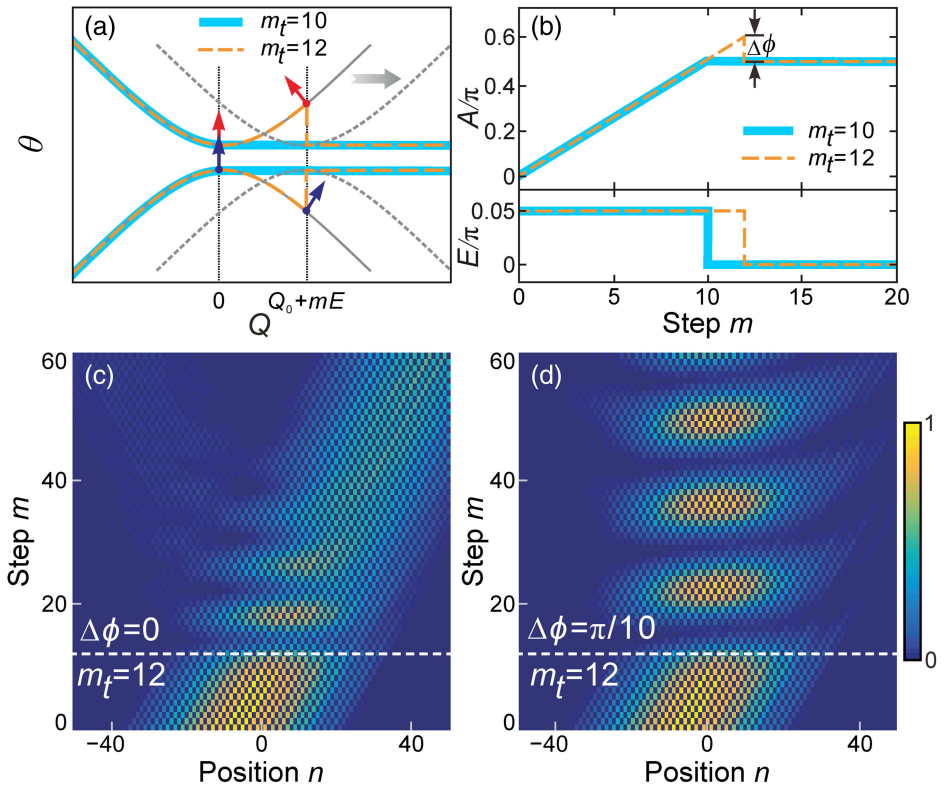

Fig. 2 Method of the measurement. (a) Band structures under the modulation of gauge potentials for the truncating time step at $m_t = 10$ and $m_t = 12$. The red (blue) arrows indicate the group velocities of the upper (lower) band during evolution. The gray arrow indicates that the band structure undergoes a horizontal displacement in the presence of effective vector potential. The dotted gray curves depict the band structure after modulation as a reference. (b) Temporal evolution of effective gauge potential and electric field for the truncation time $m_t = 10$ and $m_t = 12$. Here $\Delta\phi = (m_t - 10)E$. (c), (d) Simulated intensity profiles in the long loop for $m_t = 12$ with $\Delta\phi = 0$ (c) and $\Delta\phi = \pi/10$ (d). Here, $E = \pi/20$, $\sin^2(\beta) = 0.05$, and $\gamma = 0.1$.

change $\Delta\phi = (m_t - 10)E = \pi/10$ after the truncation, thereby making the energy bands at $m_t = 12$ turn back to the shape at the crossing point. Consequently, the two modes also exhibit an entire interference [Fig. 2(d)]. For the steps away from the band crossing point, the band occupancies can be alternatively obtained by measuring their respective intensities (Note 3 in the Supplementary Material) because the two modes are well separated in the subsequent evolution.

Figure 3(a) illustrates the measured fringes of a wave packet for the truncation at $m_t = 10$. The incident wave packet has a carrier Bloch momentum $Q_0 = -\pi/2$ and a width of $\Delta n = 15$, which can mimic an extended Bloch wave (Note 4 in the Supplementary Material).[67,68] The eigenmodes of the upper band are excited with a carrier Bloch momentum $Q_0 = -\pi/2$ by generating a Gaussian beam in short and long loops with appropriate phase and intensity relation, which is given by $|\varphi_\pm\rangle$ in Eq. (4). During interference ($m > m_t$), the evolution is

$$\begin{aligned}|\psi\rangle &= c_+|\varphi_+\rangle e^{i\theta_+ m} + c_-|\varphi_-\rangle e^{i(\theta_- m+\phi_0)}\\ &= (c_+U_+e^{i\theta_+ m} + c_-U_-e^{i(\theta_- m+\phi_0)},\\ &\quad c_+V_+e^{i\theta_+ m} + c_-V_-e^{i(\theta_- m+\phi_0)})^T\\ &= (X, Y)^T,\end{aligned}$$

where ϕ_0 denotes the phase difference of two modes and $|\varphi_\pm\rangle$ are given by Eq. (4). The normalized field intensity in the long loop reads $I(m) = |Y|^2 = (|c_+|^2 + |c_-|^2)/2 - |c_+c_-|\cos(2\beta m + \phi_0)$. According to such a relation, the band occupancies $|c_+|^2$ and $|c_-|^2$ and the phase difference ϕ_0 at $m_t + 1$ can be inversely obtained from the measured interference pattern (Note 5 in the Supplementary Material). In addition, for the truncation time $m_t = 12$ close to the crossing point $m_t = 10$, we can also observe a high contrast interference pattern after applying the abrupt change of gauge potential and get $|c_\pm|^2$ and ϕ_0 [Fig. 3(b)]. As fitted in Figs. 3(c) and 3(d), the interference patterns show high contrasts and cosine oscillations, thus evidently verifying the above analysis.

After obtaining the band occupancies at $m_t + 1$ step, we can then calculate the original band occupancies at step m_t using a retrieval method. Specifically, the modes of the adjacent time steps are connected by $|\psi\rangle = \Gamma(Q)|\psi'\rangle$ in the Q-space, where $|\psi\rangle$ and $|\psi'\rangle$ represent the modes at step $m_t + 1$ and m_t, and Γ is given by Eq. (2). At the truncation step m_t, the mode could be projected onto the eigenmode basis at step m_t, $|\psi'\rangle = c'_+|\varphi'_+\rangle + c'_-|\varphi'_-\rangle$, which can be written in a matrix form according to the eigenmodes of Eq. (4),

$$|\psi'\rangle = \begin{pmatrix} U'_+ & U'_- \\ V'_+ & V'_- \end{pmatrix}\begin{pmatrix} c'_+ \\ c'_- \end{pmatrix}. \tag{6}$$

Likewise, at the next step $m_t + 1$, the mode can be decomposed into $|\psi\rangle = c_+|\varphi_+\rangle + c_-|\varphi_-\rangle$, where $|\varphi_\pm\rangle = (U_\pm, V_\pm)^T$

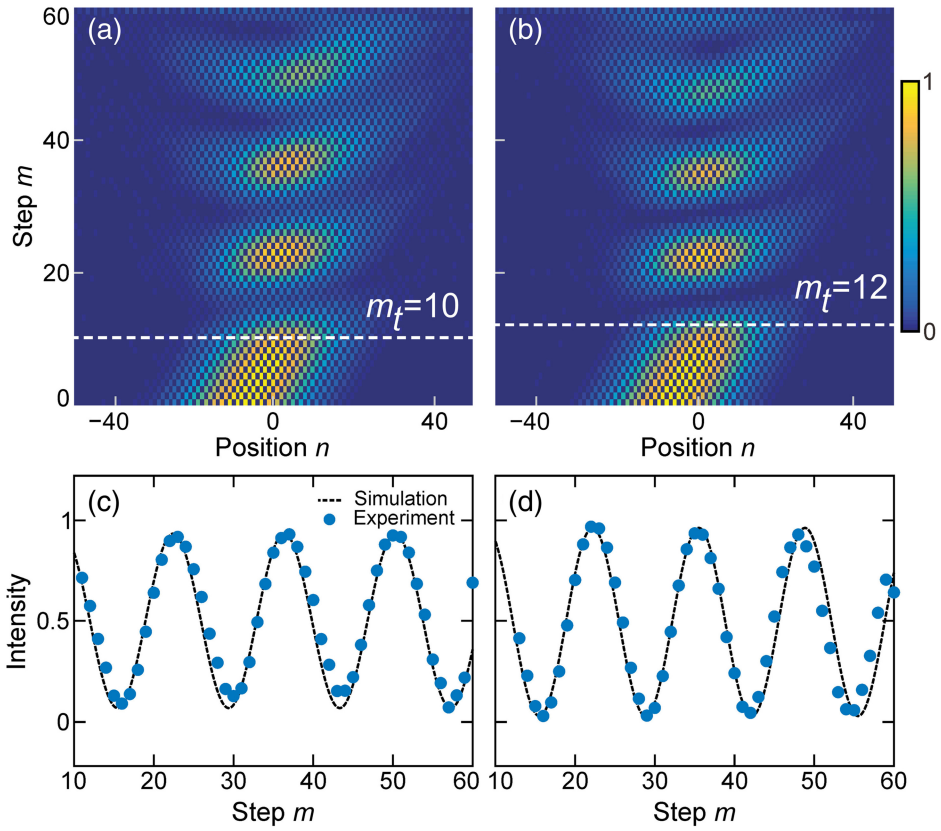

Fig. 3 Experimental interference patterns of the long loop. (a), (b) Measured interference patterns for the truncation time $m_t = 10$ (a) and $m_t = 12$ (b). An abrupt change of gauge potential $\Delta\phi = \pi/10$ is applied in the latter case. Here, $E = \pi/20$, $\sin^2(\beta) = 0.05$, and $\gamma = 0.1$ are set in experiment. (c), (d) Measured field intensities (blue dots) at each time step are shown for $m_t = 10$ (c) and $m_t = 12$ (d).

are the eigenmodes at $m_t + 1$. Also derived from Eq. (4), the mode can be expressed as

$$|\psi\rangle = \frac{1}{\sqrt{2}}\begin{pmatrix} 1 & 1 \\ 1 & -1 \end{pmatrix}\begin{pmatrix} c_+ \\ c_- \end{pmatrix}. \tag{7}$$

Considering the equation $|\psi\rangle = \Gamma(Q)|\psi'\rangle$, we can obtain the relation between the mode coefficients at m_t and $m_t + 1$, i.e.,

$$\begin{pmatrix} c'_+ \\ c'_- \end{pmatrix} = \frac{1}{\sqrt{2}}\begin{pmatrix} U'_+ & U'_- \\ V'_+ & V'_- \end{pmatrix}^{-1}\begin{pmatrix} e^{-i\beta} & e^{i\beta} \\ e^{-i\beta} & -e^{i\beta} \end{pmatrix}\begin{pmatrix} c_+ \\ c_- \end{pmatrix}. \tag{8}$$

According to Eq. (8), the band occupancies $|c'_\pm|^2$ at the truncation step can be precisely acquired by utilizing the band occupancies $|c_\pm|^2$ and the phase difference of two modes ϕ_0 after truncation. The detailed deduction is shown in Note 6 in the Supplementary Material. In fact, Eq. (8) bridges the band occupancies before and after the gauge potential variation. The connection matrix implies how the original separated modes are manipulated to form a complete interference. The original band occupancies $|c'_\pm|^2$ at time step m_t then can be obtained by the recovery algorithm based on Eq. (8).

2.3 Experimental Results of Non-Hermitian LZ Tunneling Process

Here, we experimentally demonstrate the influence of dissipation on the LZ tunneling process and show the impact of spectral phase transition on the LZ dynamics. Figures 4(a)–4(f) depict the theoretical and measured band occupancies in adiabatic bases $|c_\pm|^2$ at $\gamma = 0$, 0.1, and 0.6, accompanying the ones in diabatic bases $|c_s|^2$ and $|c_l|^2$. For the cases of $\gamma = 0$ and 0.1, the final occupancies of band θ_- (blue solid balls) and θ_l (red hollow circles) both coincide with the LZ model, which is deduced in Hermitian systems and given by $P_{\mathrm{LZ}} = \exp(-\pi\beta^2/|E|)$.[4,24,30] The reason is that the eigenmode in band θ_- is nearly identical to that in band θ_l as the tunneling completes. Meanwhile, the same paradigm is valid for the bands θ_+ and θ_s. Note that the input mode is prepared in band θ_+, and it equals the mode in band θ_l of a diabatic basis, which is always lossless in our experiment. Therefore, one still obtains

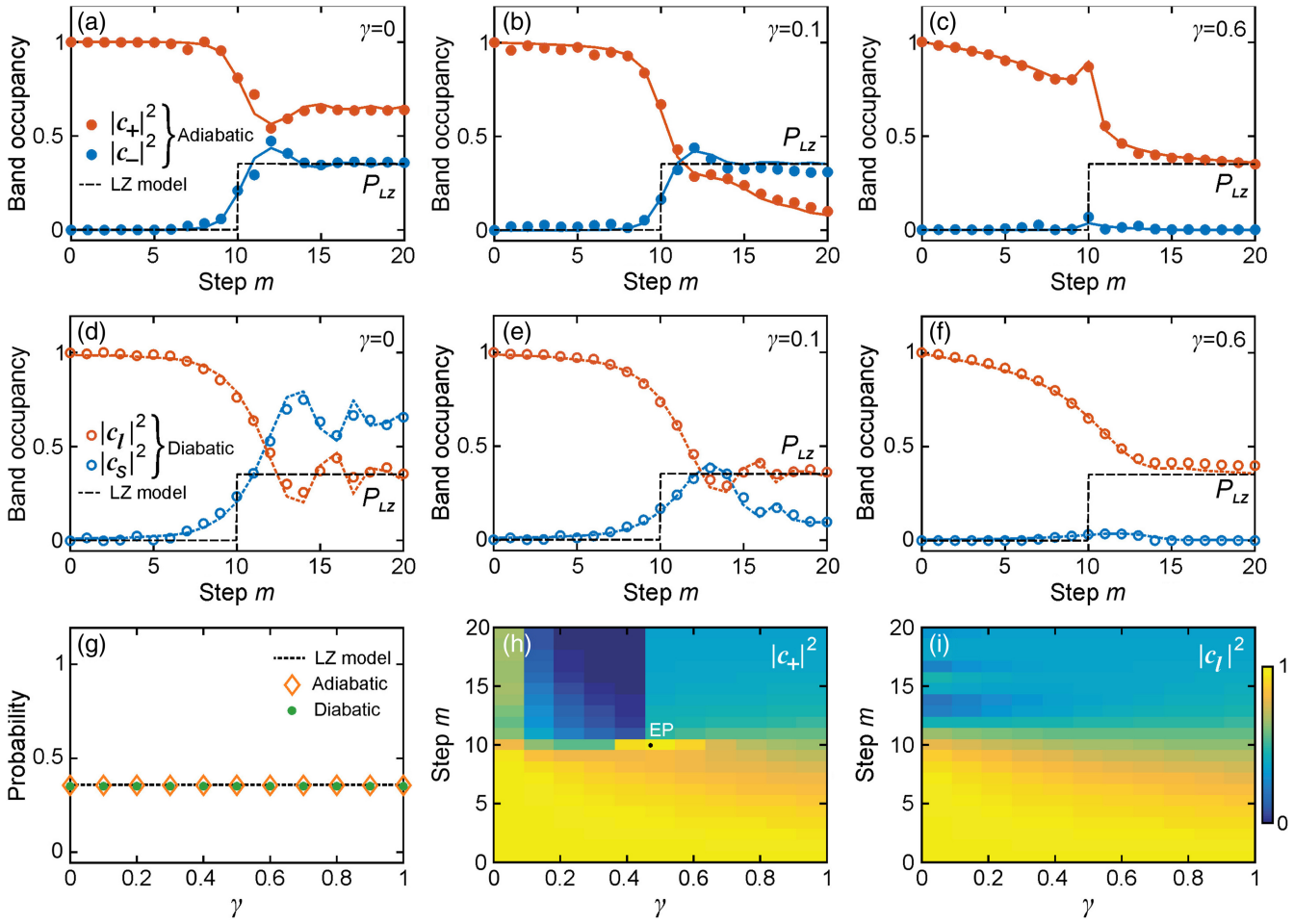

Fig. 4 Measured dynamics of non-Hermitian LZ tunneling. (a)–(c) Measured band occupancies in adiabatic basis for $\gamma = 0$, 0.1, and 0.6, respectively. (d)–(f) Same as (a)–(c) but for diabatic basis. The solid and dashed curves denote theoretical results and the experimental data are plotted in dots and circles. (g) Tunneling probabilities as a function of the loss rate in different bases. Influence of loss rate on (h) $|c_+|^2$ in adiabatic basis and (i) $|c_l|^2$ in diabatic basis. All have $E = \pi/20$ and $\sin^2(\beta) = 0.05$.

the same result predicted by the Hermitian LZ model, although the system becomes weakly non-Hermitian, say $\gamma = 0.1$ before the EP. Moreover, one can clearly observe that the characteristic oscillation of the LZ tunneling process is suppressed. The variation of the band occupancy is more rapid. The LZ dynamics change dramatically as the system turns out to be strong non-Hermitian beyond the EP. At $\gamma = 0.6$, the real bands on an adiabatic basis experience a crossing and the final modes exchange their profiles. Now, it is the mode in band θ_+ that is nearly identical to the mode in band θ_l as the tunneling completes, and the same happens to bands θ_- and θ_s, as shown in Fig. 1(c). Consequently, one sees that, according to theoretical predictions of LZ tunneling in a decaying level,[24] the occupancy of the lossless band θ_l in diabatic basis ($|c_l|^2$) still obeys LZ formula, whereas the corresponding mode belongs to band θ_+ of the adiabatic basis. The occupancies $|c_-|^2$ and $|c_s|^2$ of bands θ_- and θ_s finally remain negligible for the strong loss regime. Besides, the oscillation of the tunneling process is wearing down, and the system can quickly reach a steady state. For $\gamma = \gamma_c$, the system has an EP located at $Q = 0$, where the bands coalesce, and the eigenvectors become completely parallel. The critical value γ_c results in the ill-defined nature of the mode coefficients at EP on an adiabatic basis (see Note 2 in the Supplementary Material for a detailed derivation). Therefore, the band occupancies on an adiabatic basis are usually supposed to be the same. However, we can still measure the LZ tunneling process containing EP on a diabatic basis, which is also demonstrated in Note 2 in the Supplementary Material.

Our experiments provide the first demonstration of a rather surprising result of dissipative LZ, predicted more than three decades ago[24]: the LZ tunneling probability into a decaying level is independent of the dissipation rate. We also show the results as the loss rate varies continuously. As plotted in Fig. 4(g), we plot the tunneling probability as a function of the loss rate in adiabatic and diabatic bases. One sees that the probabilities are independent of the loss rate. We also illustrate the evolution of band occupancies in different bases as the loss rate varies. As shown in Fig. 4(h), the band occupancies in adiabatic basis decrease during the tunneling, and the process is accelerated before EP. By contrast, as shown in Fig. 4(i), the oscillation of band occupancies on a diabatic basis diminishes gradually as the loss rate increases.

To shed light on the merit of the interferometry method, we focus on the difference of total occupancies in diabatic and adiabatic bases, i.e., $(|c_l|^2 + |c_s|^2) - (|c_+|^2 + |c_-|^2)$. Such a difference should come from the non-orthogonality of eigenmodes in non-Hermitian systems. The total band occupancies of $|c_+|^2 + |c_-|^2$ in adiabatic basis and $|c_l|^2 + |c_s|^2$ in diabatic basis are both shown in Figs. 5(a) and 5(b) for different loss rates. As $\gamma = 0$, both occupancies are conserved as the system is Hermitian, whereas the difference appears near the band crossings for $\gamma > 0$. The total occupancy in the diabatic basis represents the total energy in the two loops as the two basis vectors are orthogonal. The attenuation of total occupancy with time indicates the energy loss during evolution. Considering the non-orthogonality of eigenmodes on the adiabatic basis, the total occupancy cannot be represented by energy. Figure 5(c) illustrates the modulus of the inner product $\langle\varphi_+|\varphi_-\rangle$ in the parameter space spanned by Q and γ. For the Hermitian case with $\gamma = 0$, the product is 0. In addition, the eigenmodes are almost orthogonal in the regions away from the band crossings ($Q = 0$). This is because the mode profiles are distributed separately in the long and short loops when approaching the Brillouin zone edges. The maximum value of the product is

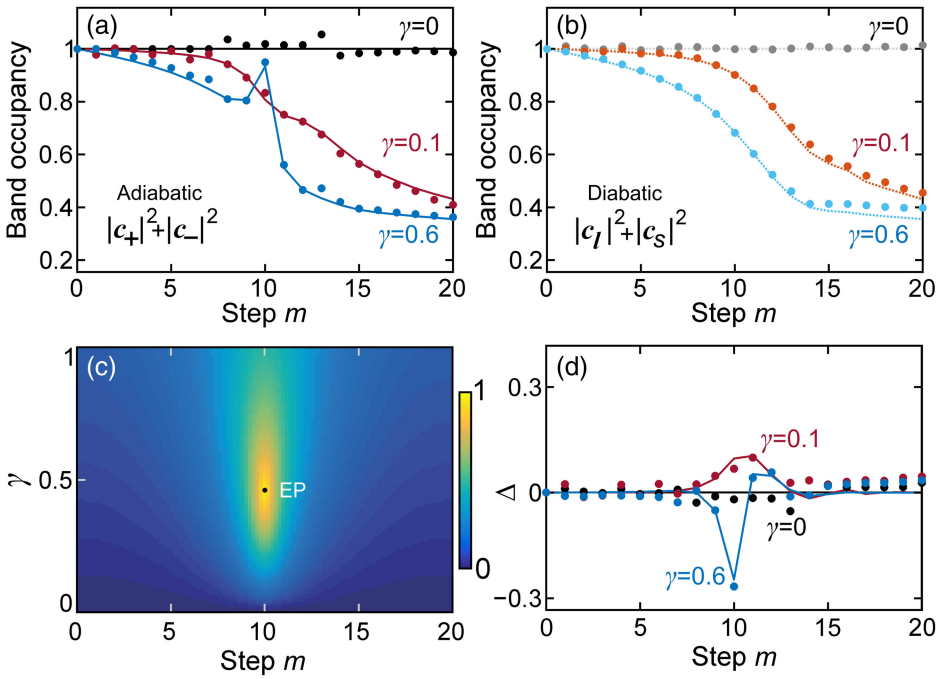

Fig. 5 Non-orthogonality of eigenmodes. (a), (b) Total band occupancies in adiabatic (a) and diabatic (b) bases. (c) Overlap of the eigenmodes $|\langle\varphi_+|\varphi_-\rangle|$ in dependence on step m and loss rate γ. (d) Deviation of the total band occupancies in different bases. The solid curves represent the theoretical results, and the experimental data are plotted in dots.

located rightly at the EP, showing the most difference between the two bases. The theoretical difference of the total occupancies should be $\Delta = (|c_l|^2 + |c_s|^2) - (|c_+|^2 + |c_-|^2) = 2\,\mathrm{Re}(c_+^* c_- \langle\varphi_+|\varphi_-\rangle)$ according to the inner product $\langle\varphi_+|\varphi_-\rangle$ represented in adiabatic basis. The corresponding experimental results of difference are obtained by calculating the difference of the measured total occupancies in different bases, which is plotted in Fig. 5(d), indicating that the band occupancies in adiabatic basis are not equivalent to energy, especially near the avoided crossings. Therefore, one has to measure both the amplitude and phase of the mode coefficients. The interferometry method proposed here provides an effective way to measure the occupancies of the non-Hermitian system remaining all the information.

3 Conclusion

We have experimentally demonstrated non-Hermitian LZ tunneling for complex energy bands using temporal photonic lattices and unveiled the major role of dissipation in tunneling dynamics. To accurately determine the tunneling process, we harnessed a stepwise quench method and extracted the real-time band occupancies from mode interferences. Our measurements revealed that dissipation does not change the final LZ tunneling probability; however, it can remarkably influence the transient process of LZ tunneling. As the loss rate crosses EPs from weak to strong non-Hermitian regimes, the characteristic oscillations can be smeared out, thereby speeding up LZ tunneling and leading to quicker achievement of steady band occupancies. In addition, we demonstrated that the non-orthogonality of eigenmodes in non-Hermitian systems can make the total band occupancy diverge from the real energy in the LZ tunneling process. Our experimental results unravel the intriguing LZ physics and LZ interferometry beyond the standard Hermitian paradigm, which could be of main relevance in the broad and timely research area of non-Hermitian physics with potential applications to coherent quantum control and modern quantum technologies.[27]

Disclosures

The authors declare no competing interests.

Code and Data Availability

All the data supporting this study are available in the paper and Supplementary Material. Additional data related to this paper are available from the corresponding authors upon request.

Acknowledgments

This work is supported by the National Natural Science Foundation of China [Grant Nos. 12374305 (B.W.), 12474381 (C.Q.), 12021004 (P.L.), 62305122 (S.W.), 12204185 (C.Q.), and 62375097 (W.L.)]. S.L. acknowledges the Spanish Agencia Estatal de Investigacion (Grant No. MDM-2017-0711).

References

1. C. Zener, "Non-adiabatic crossing of energy levels," *Proc. R. Soc. Lond. A* **137**, 696–702 (1932).
2. L. D. Landau, "Theorie der Energieubertragung. II," *Phys. Z. Sowjetunion* **2**, 46 (1932).
3. N. V. Vitanov, "Transition times in the Landau–Zener model," *Phys. Rev. A* **59**, 988–994 (1999).
4. O. V. Ivakhnenko, S. N. Shevchenko, and F. Nori, "Nonadiabatic Landau–Zener–Stückelberg–Majorana transitions, dynamics, and interference," *Phys. Rep.* **995**, 1–89 (2023).
5. P. Voisin et al., "Observation of the Wannier–Stark quantization in a semiconductor superlattice," *Phys. Rev. Lett.* **61**, 1639–1642 (1988).
6. J. Feldmann et al., "Optical investigation of Bloch oscillations in a semiconductor superlattice," *Phys. Rev. B* **46**, 7252–7255 (1992).
7. S. R. Wilkinson et al., "Observation of atomic Wannier–Stark ladders in an accelerating optical potential," *Phys. Rev. Lett.* **76**, 4512–4515 (1996).
8. B. P. Anderson and M. A. Kasevich, "Macroscopic quantum interference from atomic tunnel arrays," *Science* **282**, 1686–1689 (1998).
9. W. D. Oliver et al., "Mach–Zehnder interferometry in a strongly driven superconducting qubit," *Science* **310**, 1653–1657 (2005).
10. M. Ghulinyan et al., "Zener tunneling of light waves in an optical superlattice," *Phys. Rev. Lett.* **94**, 127401 (2005).
11. H. Trompeter et al., "Bloch oscillations and Zener tunneling in two-dimensional photonic lattices," *Phys. Rev. Lett.* **96**, 053903 (2006).
12. H. Sanchis-Alepuz, Y. A. Kosevich, and J. Sánchez-Dehesa, "Acoustic analogue of electronic Bloch oscillations and resonant Zener tunneling in ultrasonic superlattices," *Phys. Rev. Lett.* **98**, 134301 (2007).
13. E. H. Hauge and J. A. Støvneng, "Tunneling times: a critical review," *Rev. Mod. Phys.* **61**, 917–936 (1989).
14. K. Mullen et al., "Time of Zener tunneling," *Phys. Rev. Lett.* **62**, 2543–2546 (1989).
15. R. Landauer and T. Martin, "Barrier interaction time in tunneling," *Rev. Mod. Phys.* **66**, 217–228 (1994).
16. F. Dreisow et al., "Bloch–Zener oscillations in binary superlattices," *Phys. Rev. Lett.* **102**, 076802 (2009).
17. A. Zenesini et al., "Time-resolved measurement of Landau–Zener tunneling in periodic potentials," *Phys. Rev. Lett.* **103**, 090403 (2009).
18. C. M. Bender, "Making sense of non-Hermitian Hamiltonians," *Rep. Prog. Phys.* **70**, 947 (2007).
19. N. Moiseyev, *Non-Hermitian Quantum Mechanics*, Cambridge University Press (2011).
20. Y. Ashida, Z. Gong, and M. Ueda, "Non-Hermitian physics," *Adv. Phys.* **69**, 249–435 (2020).
21. N. Bender et al., "Wave-packet self-imaging and giant recombinations via stable Bloch–Zener oscillations in photonic lattices with local PT symmetry," *Phys. Rev. A* **92**, 041803 (2015).
22. M. Wimmer et al., "Observation of Bloch oscillations in complex PT-symmetric photonic lattices," *Sci. Rep.* **5**, 17760 (2015).
23. Y. L. Xu et al., "Experimental realization of Bloch oscillations in a parity-time synthetic silicon photonic lattice," *Nat. Commun.* **7**, 11319 (2016).
24. V. M. Akulin and W. P Schleich, "Landau–Zener transition to a decaying level," *Phys. Rev. A* **46**, 4110–4113 (1992).
25. N. V. Vitanov and S. Stenholm, "Pulsed excitation of a transition to a decaying level," *Phys. Rev. A* **55**, 2982–2988 (1997).
26. E. M. Graefe and H. J. Korsch, "Crossing scenario for a nonlinear non-Hermitian two-level system," *Czech. J. Phys.* **56**, 1007–1020 (2006).
27. K. Saito et al., "Dissipative Landau–Zener transitions of a qubit: bath-specific and universal behavior," *Phys. Rev. B* **75**, 214308 (2007).
28. B. T. Torosov, G. Della Valle, and S. Longhi, "Non-Hermitian shortcut to adiabaticity," *Phys. Rev. A* **87**, 052502 (2013).
29. Y. Avishai and Y. B. Band, "Landau–Zener problem with decay and dephasing," *Phys. Rev. A* **90**, 032116 (2014).

30. B. T. Torosov and N. V. Vitanov, "Pseudo-Hermitian Landau–Zener–Stückelberg–Majorana model," *Phys. Rev. A* **96**, 013845 (2017).
31. Z.-Y. Ge et al., "Topological band theory for non-Hermitian systems from the Dirac equation," *Phys. Rev. B* **100**, 054105 (2019).
32. S. Longhi, "Non-Bloch-band collapse and chiral Zener tunneling," *Phys. Rev. Lett.* **124**, 066602 (2020).
33. R. Melanathuru, S. Malzard, and E.-M. Graefe, "Landau–Zener transitions through a pair of higher-order exceptional points," *Phys. Rev. A* **106**, 012208 (2022).
34. B. Longstaff and E.-M. Graefe, "Nonadiabatic transitions through exceptional points in the band structure of a PT-symmetric lattice," *Phys. Rev. A* **100**, 052119 (2019).
35. X. Shen et al., "Landau–Zener–Stückelberg interferometry in PT-symmetric non-Hermitian models," *Phys. Rev. A* **100**, 062514 (2019).
36. J.-S. Pan and F. Wu, "Nonadiabatic transitions in non-Hermitian PT-symmetric two-level systems," *Phys. Rev. A* **109**, 022245 (2024).
37. M. V. Berry, "Physics of non-Hermitian degeneracies," *Czech. J. Phys.* **54**, 1039–1047 (2004).
38. W. D. Heiss, "The physics of exceptional points," *J. Phys. A: Math. Theor.* **45**, 444016 (2012).
39. M.-A. Miri and A. Alù, "Exceptional points in optics and photonics," *Science* **363**, eaar7709 (2019).
40. Ş. K. Özdemir et al., "Parity-time symmetry and exceptional points in photonics," *Nat. Mater.* **18**, 783–798 (2019).
41. M. V. Berry and R. Uzdin, "Slow non-Hermitian cycling: exact solutions and the Stokes phenomenon," *J. Phys. A: Math. Theor.* **44**, 435303 (2011).
42. J. Doppler, et al., "Dynamically encircling an exceptional point for asymmetric mode switching," *Nature* **537**, 76–79 (2016).
43. J. Alexandre and C. M. Bender, "Foldy-Wouthuysen transformation for non-Hermitian Hamiltonians," *J. Phys. A: Math. Theor.* **48**, 185403 (2015).
44. S. Longhi, "Non-Hermitian topological phase transitions in superlattices and the optical Dirac equation," *Opt. Lett.* **46**, 4470–4473 (2021).
45. A. Regensburger et al., "Photon propagation in a discrete fiber network: an interplay of coherence and losses," *Phys. Rev. Lett.* **107**, 233902 (2011).
46. A. Regensburger et al., "Parity-time synthetic photonic lattices," *Nature* **488**, 167–171 (2012).
47. M. Wimmer et al., "Experimental measurement of the Berry curvature from anomalous transport," *Nat. Phys.* **13**, 545–550 (2017).
48. S. Weidemann et al., "Topological funneling of light," *Science* **368**, 311–314 (2020).
49. M. Wimmer et al., "Superfluidity of light and its breakdown in optical mesh lattices," *Phys. Rev. Lett.* **127**, 163901 (2021).
50. S. Wang et al., "High-order dynamic localization and tunable temporal cloaking in ac-electric-field driven synthetic lattices," *Nat. Commun.* **13**, 7653 (2022).
51. S. Weidemann et al., "Topological triple phase transition in non-Hermitian Floquet quasicrystals," *Nature* **601**, 354–359 (2022).
52. S. Wang et al., "Photonic Floquet Landau–Zener tunneling and temporal beam splitters," *Sci. Adv.* **9**, eadh0415 (2023).
53. H. Ye et al., "Reconfigurable refraction manipulation at synthetic temporal interfaces with scalar and vector gauge potentials," *Proc. Natl. Acad. Sci. U. S. A* **120**, e2300860120 (2023).
54. C. Qin et al., "Spectrum control through discrete frequency diffraction in the presence of photonic gauge potentials," *Phys. Rev. Lett.* **120**, 133901 (2018).
55. A. Dutt et al., "Experimental band structure spectroscopy along a synthetic dimension," *Nat. Commun.* **10**, 3122 (2019).
56. K. Wang et al., "Topological complex-energy braiding of non-Hermitian bands," *Nature* **598**, 59–64 (2021).
57. K. Wang et al., "Generating arbitrary topological windings of a non-Hermitian band," *Science* **371**, 1240–1245 (2021).
58. F. Cardano et al., "Detection of Zak phases and topological invariants in a chiral quantum walk of twisted photons," *Nat. Commun.* **8**, 15516 (2017).
59. X. W. Luo et al., "Synthetic-lattice enabled all-optical devices based on orbital angular momentum of light," *Nat. Commun.* **8**, 16097 (2017).
60. L. Yuan et al., "Synthetic dimension in photonics," *Optica* **5**, 1396–1405 (2018).
61. E. Lustig et al., "Photonic topological insulator in synthetic dimensions," *Nature* **567**, 356–360 (2019).
62. M. Ehrhardt et al., "A perspective on synthetic dimensions in photonics," *Laser Photonics Rev.* **17**, 2200518 (2023).
63. K. Fang, Z. Yu, and S. Fan, "Photonic Aharonov–Bohm effect based on dynamic modulation," *Phys. Rev. Lett.* **108**, 153901 (2012).
64. Q. Lin and S. Fan, "Light guiding by effective gauge field for photons," *Phys. Rev. X* **4**, 031031 (2014).
65. S. Ibáñez and J. G. Muga, "Adiabaticity condition for non-Hermitian Hamiltonians," *Phys. Rev. A* **89**, 033403 (2014).
66. K. Kawabata et al., "Symmetry and topology in non-Hermitian physics," *Phys. Rev. X* **9**, 041015 (2019).
67. A. Steinfurth et al., "Observation of photonic constant-intensity waves and induced transparency in tailored non-Hermitian lattices," *Sci. Adv.* **8**, eabl7412 (2022).
68. T. Eichelkraut et al., "Mobility transition from ballistic to diffusive transport in non-Hermitian lattices," *Nat. Commun.* **4**, 2533 (2013).

Lange Zhao received her BS degree from the School of Physics, Huazhong University of Science and Technology, China in 2019. She is currently a PhD student at Huazhong University of Science and Technology. Her research interests focus on nanophotonics and non-Hermitian physics.

Shulin Wang received his PhD from the School of Physics, Huazhong University of Science and Technology, Wuhan, China in 2021. He is currently an associate research fellow at School of Physics, Southeast University. His current research interests include synthetic dimension, non-Hermitian physics and nonlinear optics.

Chengzhi Qin received his BS degree in optics and electronic information and PhD in physics from Huazhong University of Science and Technology, Wuhan, China in 2014 and 2019, respectively. He is currently an associate professor at the School of Physics, Huazhong University of Science and Technology. His research interests include topological photonics, nanophotonics and non-Hermitian physics.

Bing Wang received his BS and PhD in physics from Wuhan University, Wuhan, China in 2002 and 2007, respectively. He is currently a professor at the School of Physics and Wuhan National Laboratory for Optoelectronics, Huazhong University of Science and Technology, Wuhan, China. His research interests include metal/graphene plasmonics, nanophotonics, nonlinear and ultrafast optics.

Han Ye received his BS and PhD degrees from the School of Physics, Huazhong University of Science and Technology, China in 2018 and 2023, respectively. His research interests focus on nanophotonics and non-Hermitian physics.

Weiwei Liu received his BS and PhD degrees in optics and electronic information both from Huazhong University of Science and Technology, Wuhan, China in 2012 and 2017, respectively. He is currently an associate professor at the School of Physics, Huazhong University of Science and Technology. His research interests include nonlinear optics, nanophotonics and topological photonics.

Stefano Longhi received his PhD in physics from Polytechnic Institute of Turin (with distinguished honor) in 1996. He is currently a full professor of Physics Department, Polytechnic Institute of Milan and research associate with IFISC, University of the Balearic Islands, Palma de Mallorca (Spain). His research interests include photonics, quantum optics, and non-Hermitian physics.

Peixiang Lu received his PhD from the Shanghai Institute of Optics and Fine Mechanics, Chinese Academy of Sciences, Shanghai, in 1992. He is currently a professor at Wuhan National Laboratory for Optoelectronics, Huazhong University of Science and Technology. He is a fellow of Optica. His current research interests include ultrafast optics, laser physics, and nanophotonics.